Nonlinear distortion of short pulses radiated by plane and focused circular pistons

Michalakis A. Averkiou
Applied Physics Laboratory, University of Washington, Seattle, Washington 98105

Mark F. Hamilton
Department of Mechanical Engineering, The University of Texas at Austin, Austin, Texas 78712-1063

(Received 19 June 1996; accepted for publication 2 June 1997)

Detailed measurements of finite-amplitude pulses radiated by plane and focused circular pistons in water are presented. Comparisons of time waveforms and frequency spectra, both on and off axis, are made with numerical calculations based on the nonlinear parabolic wave equation. Emphasis is on nonlinear distortion of amplitude- and frequency-modulated tone bursts. Use of short pulses enabled resolution of the direct and diffracted waves prior to their coalescence and subsequent shock formation along the axis of the source. Because of its relevance to investigations of cavitation inception, attention is devoted to variation of the peak positive (p_+) and negative (p_-) pressures along the axis of a focused source. It is shown that with increasing source amplitude, the maximum of each shifts away from the focal plane, toward the source. This effect is more pronounced for p_- than for p_+. © *1997 Acoustical Society of America.* [S0001-4966(97)06110-9]

PACS numbers: 43.25.Ts, 43.80.Sh [MAB]

INTRODUCTION

The use of intense ultrasound in medical and industrial applications has increased considerably in recent years. Both plane and focused sources are used widely in either continuous wave (cw) or pulsed mode, and at intensities which lead to nonlinear effects such as harmonic generation and shock formation. Typical ultrasonic sources generate strong diffraction phenomena, which combine with finite amplitude effects to produce waveforms that vary from point to point within the sound beam. Nonlinear effects have become especially important at acoustic intensities employed in many current therapeutic and surgical procedures.[1] In addition, biological media can introduce significant absorption of sound, which must also be considered.

The emphasis of the present article is on detailed comparisons of theory and experiment for pulsed finite-amplitude sound beams radiated from plane and focused circular pistons. Comparisons of theory and experiment for the case of small-signal transient radiation from plane circular pistons have been reviewed by Hutchins and Hayward.[2] Similar comparisons for the case of focused circular pistons have also been reported, with perhaps the first extensive investigation of this kind described in the article by Goodsitt *et al.*[3] More recently, Djelouah *et al.*[4,5] compared theory with measurements of sufficiently short pulses that the direct and diffracted wave contributions along the axis were easily resolved.

The first comparisons of an appropriate theoretical model with measurements of pulsed finite-amplitude sound beams containing shocks are presented in the work by Baker and Humphrey.[6–8] They compared measurements of short pulses (one cycle excitation that resulted in roughly three cycles due to the bandwidth of the source) at finite amplitudes with results from a finite difference algorithm that solves the KZK (Khokhlov–Zabolotskaya–Kuznetsov) nonlinear parabolic wave equation.[9,10] They investigated pulses radiated by plane circular pistons in Ref. 6, by focused circular pistons in Ref. 7, and by both varieties in Ref. 8. A frequency domain algorithm was used to solve the KZK equation, which required repetition of each pulse periodically in time to represent the signal in terms of a discrete Fourier series.

The purpose of the present article is to compare measurements of pulsed finite amplitude sound beams in water, both focused and unfocused, with predictions obtained from a time domain algorithm for solving the KZK equation. The investigation also differs from those reported by Baker and Humphrey[6–8] principally in terms of greater breadth and precision. Both amplitude- and frequency-modulated tone bursts are considered, coalescence and interference of direct and edge waves are reported, and the likelihood of preferential sites for acoustic cavitation[11] in a focused sound beam is investigated with measurements and calculations of negative pressure excursions along the axis of the beam.

I. THEORY

The theoretical predictions in Sec. III are obtained from numerical solutions of the KZK nonlinear parabolic wave equation, written here in terms of the sound pressure p:

$$\frac{\partial^2 p}{\partial z\,\partial t'} = \frac{c_0}{2}\left(\frac{\partial^2 p}{\partial r^2} + \frac{1}{r}\frac{\partial p}{\partial r}\right) + \frac{\delta}{2c_0^3}\frac{\partial^3 p}{\partial t'^3} + \frac{\beta}{2\rho_0 c_0^3}\frac{\partial^2 p^2}{\partial t'^2}. \tag{1}$$

Only axisymmetric radiation is considered, with z the coordinate along the axis of the sound beam, r the distance from the beam axis, and $t' = t - z/c_0$ a retarded time, where c_0 is the propagation speed. The first term on the right-hand side of Eq. (1) accounts for diffraction. Thermoviscous attenuation is taken into account by the second term, where δ is the sound diffusivity.[12] In the third term, $\beta = 1 + B/2A$ is the

coefficient of nonlinearity[13] and ρ_0 is the ambient density of the fluid. In general, Eq. (1) is an accurate model of the sound field produced by directional sound sources ($ka \gg 1$, where k characterizes the wave number and a the radius of the source) at distances beyond a few source radii and in regions close to the axis of the source, the paraxial region (up to about 20° off the z axis in the far field). These restrictions are satisfied in most practical applications of directional sound beams. A complete discussion of the domain of validity of the KZK equation for plane and focused piston sources is provided in Refs. 14 and 15.

Two source conditions are considered, one for plane and the other for focused circular radiators, each with uniform velocity amplitude and radius a. For the plane circular sources we prescribe the boundary condition

$$p = p_0 E(t) \sin[\omega_0 t + \phi(t)] H(1 - r/a) \quad \text{at } z = 0, \tag{2}$$

where p_0 is the effective pressure amplitude at the source, $E(t)$ and $\phi(t)$ are amplitude and phase modulations, respectively, of a signal at angular frequency ω_0 (in all calculations and experiments, $f_0 = \omega_0/2\pi$ is the resonance frequency of the transducer), and H is the Heaviside unit step function. Since the order of accuracy of the KZK equation is consistent with the use of the linear plane wave impedance relation[16] $p = \rho_0 c_0 u$, where u is the particle velocity in the z direction, we have used this relation to express the boundary condition (2) in terms of pressure rather than particle velocity. For the envelope function we define

$$E(t) = \exp[-(2t/T)^{2m}], \tag{3}$$

where T characterizes its duration and m its rise and decay time. The instantaneous angular frequency of the signal is $\Omega(t) = \omega_0 + d\phi/dt$.

Numerical solutions of Eq. (1) subject to Eq. (2) were obtained using finite difference algorithms. With the exception of the predictions in Fig. 2 for continuous radiation from a plane circular piston, which were calculated with the spectral code described by Naze Tjøtta *et al.*,[15] all calculations were performed with the time domain code described by Lee and Hamilton.[17] An advantage of the spectral code is that propagation in media with arbitrary attenuation and dispersion can be modeled. However, only thermoviscous attenuation, as described by Eq. (1), need be considered for the experiments reported in the present article. As discussed by Cleveland *et al.*,[18] absorption and dispersion due to multiple relaxation phenomena can also be included in the time domain code. An advantage of the time domain code is its suitability for modeling pulses, random signals, and shock rise times. An early listing of the time domain code is provided by Lee.[19]

Given the boundary condition in Eq. (2), the solutions of Eq. (1) are determined completely (numerical error notwithstanding) by the following two independent dimensionless parameters:

$$A_u = \alpha_0 z_0, \quad N_u = z_0/\overline{z}. \tag{4}$$

The subscript u, and subsequently f, is used to distinguish between the parameters for unfocused (plane) and focused sources, respectively. Both parameters in Eqs. (4) are normalized by the Rayleigh distance $z_0 = \omega_0 a^2/2c_0$. In the definition of the absorption parameter A_u, $\alpha_0 = \delta\omega_0^2/2c_0^3$ is the thermoviscous attenuation coefficient at frequency ω_0. Thus, A_u is the ratio of the characteristic diffraction and absorption length scales. In the nonlinearity parameter N_u, $\overline{z} = \rho_0 c_0^3/\beta\omega_0 p_0$ is the plane wave shock formation distance, and therefore N_u is the ratio of the characteristic diffraction and nonlinearity length scales.

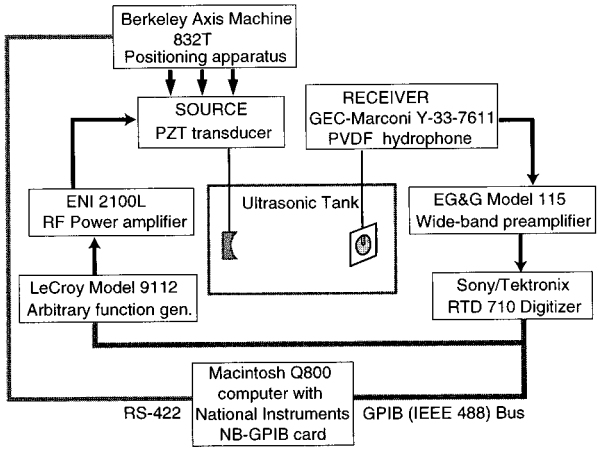

FIG. 1. Block diagram of the experimental setup.

For a focused source with focal length d we replace t with $t + r^2/2c_0 d$ in Eq. (2). The code as listed by Lee[19] for plane, diverging sound beams was modified to accommodate the geometry of focused beams. Three dimensionless parameters must now be specified:

$$G = z_0/d, \quad A_f = \alpha_0 d, \quad N_f = d/\overline{z}, \tag{5}$$

where G is the linear focusing gain, equal to the peak value of p/p_0 at the geometric focus $(r,z) = (0,d)$ for continuous small-signal radiation at frequency ω_0 in a lossless fluid. The absorption parameter A_f and nonlinearity parameter N_f are scaled here according to the focal length.

II. EXPERIMENT

A block diagram of the experimental setup is shown in Fig. 1. The measurements were made in the ultrasonics water tank described previously by TenCate[20] (see also Ref. 21). Positioning and movement of the sources with respect to the hydrophone was accomplished with a Berkeley Axis Machine 832T (20-μm spatial resolution).

Two different plane sources were used, both made by Panametrics. One has an effective radius $a = 9.4$ mm and a center resonance frequency $f_0 = 2.25$ MHz, and the other has an effective radius $a = 12.1$ mm and a center resonance frequency $f_0 = 1$ MHz. The effective radius of the source was determined by comparing measurements of far-field beam patterns with linear theory. The corresponding Rayleigh distances are $z_0 = 420$ mm and $z_0 = 310$ mm, respectively (the measured sound speed in the water was $c_0 = 1486$ m/s).

We used the same focused source, manufactured by Harisonic, as in experiments on cw radiation reported earlier.[22] Focusing was achieved not with a lens, but by hav-

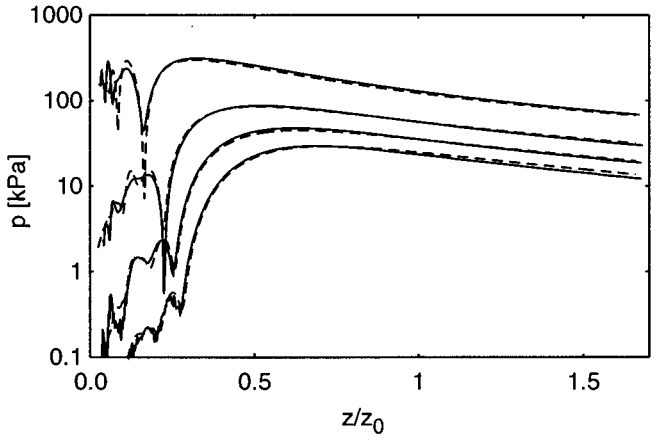

FIG. 2. Comparison of experiment (solid lines; $f_0=2.25$ MHz, $a=9.4$ mm, $z_0=420$ mm) and theory (dashed lines; $A_u=0.053$, $N_u=0.97$) for the pressure amplitudes of the lowest four harmonic components (fundamental through fourth harmonic in top to bottom order) in a plane piston beam.

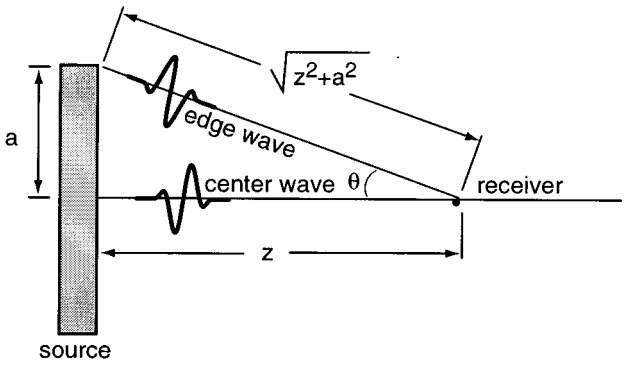

FIG. 3. Geometry of direct and diffracted wave arrivals.

ing the PZT transducer cut to form a spherical concave surface. As described in the previous work,[22] the effective radius and focal length of the source were determined to be $a=18.8$ mm and $d=160$ mm, respectively. When driven continuously at 2.25 MHz, the focusing gain is $G=10.5$.

A LeCroy model 9112 arbitrary function generator was used to generate the source waveforms, and an ENI 2100L RF power amplifier was used to amplify the signal to the sources. The receive system is identical to that employed in the earlier experiments.[22] We used a bilaminar Marconi PVDF membrane hydrophone (1-mm active diameter, 25-μm film thickness). This type of hydrophone has a resonance frequency at about 23 MHz, and its sensitivity falls off above that frequency.[23] The hydrophone was calibrated at National Physical Laboratory (Teddington, UK), and the reported variation of sensitivity with frequency was factored out of the measurements. The hydrophone signal was amplified with an EG&G model 15 wide-band preamplifier (50-MHz cutoff frequency), and sampled with a Sony/Tektronix RTD 710 digitizer (10 bit) at a rate of 200 MHz. Dynamic range was improved by repeated averaging of the received signals, typically 1024 times.

III. RESULTS

In this section we present our experimental results and compare them with theoretical predictions. We divide our results in two categories, plane pistons and focused pistons. We begin with the plane pistons.

A. Plane pistons

In order to compare measured waveforms with the theoretical model we first ensure that the source behaves as a circular piston, as assumed in accordance with Eq. (2). In Fig. 2 we show measurements of an axial propagation curve produced by continuous radiation from the plane 2.25-MHz source (solid lines), and theoretical predictions (dashed lines) based on a code that solves the KZK equation in the frequency domain[15] (all other calculations in this article are obtained from a time domain code[17]). The absorption and nonlinearity parameters used in the theoretical model are $A_u=0.053$ and $N_u=0.97$, respectively. The first four harmonics are shown. From Fig. 2 we see that there is excellent agreement between measurement and theory over a dynamic range of about 70 dB. Measured axial propagation curves for the 1-MHz source exhibited similar agreement with theory. We thus conclude that our sources behave as nearly ideal pistons, and we proceed to our measurements of pulses.

A circular piston is excited with a short pulse (a couple of cycles), and the field at a distance z along the axis of the source is monitored as shown in Fig. 3. Very near the source, two distinct contributions to the received signal can be identified. The first is called the direct wave (or center wave), because its arrival time is equal to that of a signal originating from the exact center of the source. The second is called the diffracted wave (or edge wave), because its arrival time corresponds to that of a wave radiated at the edge of the source. The direct wave arrives first after traveling a distance z, and the diffracted wave, an inverted replica of the direct wave, arrives second after traveling a distance $\sqrt{z^2+a^2}$. The difference in arrival times approaches zero far away from the source. Small-signal theory and experiments related to these effects are reviewed by Hutchins and Hayward.[2]

In Fig. 4 we show measured time waveforms for a short pulse at various positions along the axis of the source. The 2.25-MHz source was excited with a single cycle at that frequency, but due to bandwidth limitations of the source the waveform actually radiated was longer (approximately 2 cycles). At $z=2$ mm, the measurement location nearest to the source, the direct wave is clearly seen (first arrival), but the edge wave (second arrival) is difficult to distinguish. In general, as observed by others,[2] the measured edge waves shown in the first column change considerably from one location to the next because of the directivity of the hydrophone. The angles $\theta=\arctan(a/z)$ given in the figure correspond to the angle formed by the axis of the source and the line that passes through the axial observation point and the edge of the circular source (see Fig. 3). As indicated by the measurements of directivities reported by Bacon,[23] the sensitivity of a membrane hydrophone having an active element 1 mm in diameter may be expected to vary dramatically at 2.25 MHz through the range of angles in the first column of

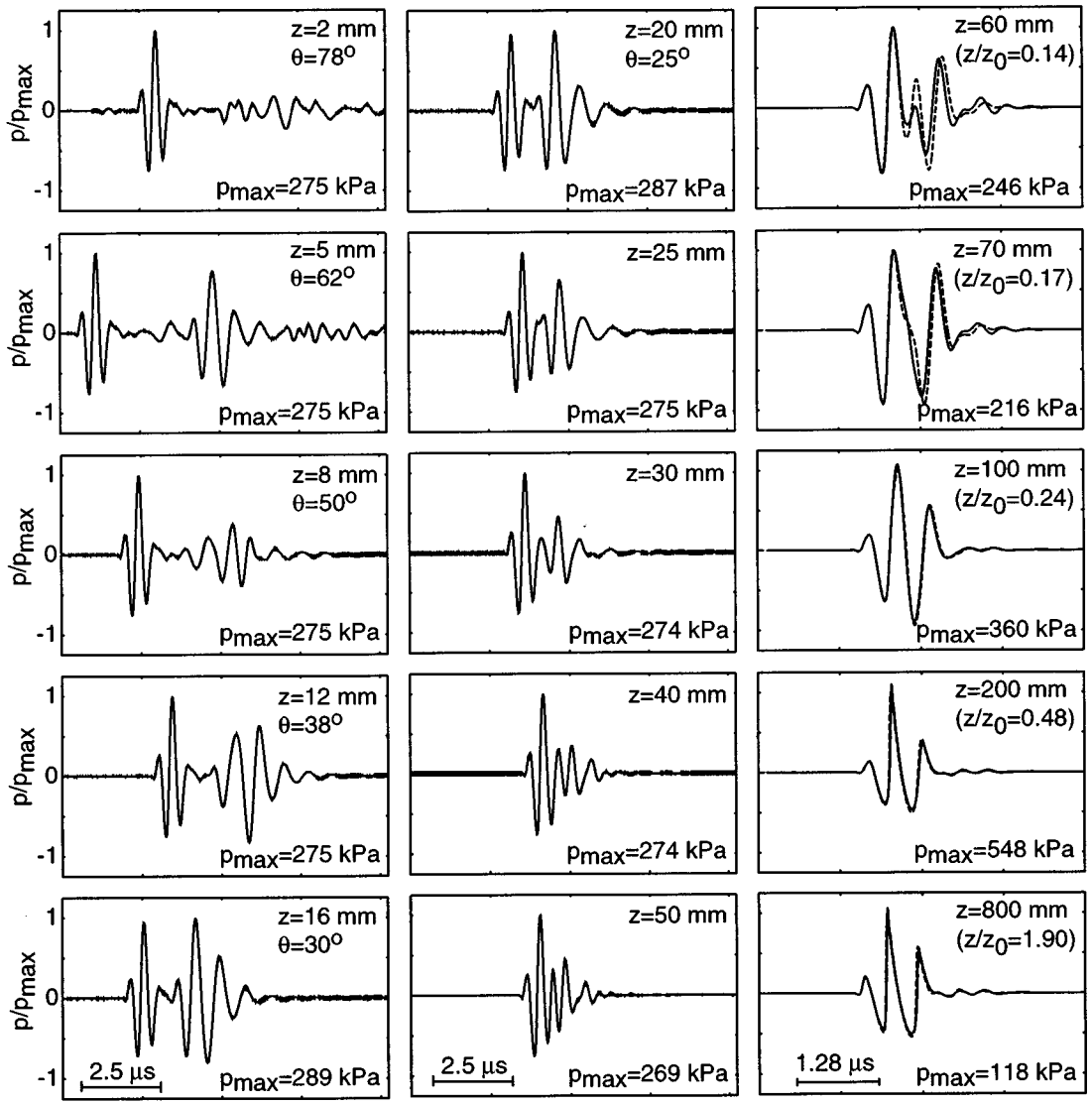

FIG. 4. Measurements (solid lines; $f_0=2.25$ MHz, $a=9.4$ mm, $z_0=420$ mm) of a short pulse along the axis of a plane piston, and comparison with theory (dashed lines in third column; $A_u=0.053$, $N_u=1.72$).

Fig. 4. In particular, subsequent measurements[24] show that at 2 MHz the hydrophone used in our experiments has a full-width half-angle, where the first null appears, of approximately 43°.

The second and third columns in Fig. 4 show the coalescence of the direct and edge waves in the region from $z=25$ mm to $z=100$ mm, where finite amplitude effects on the wave remain minor. Between $z=100$ mm and $z=200$ mm the effect of nonlinearity becomes pronounced, and a shock is formed in the center of the pulse. The distortion increases further out to $z=800$ mm.

In the third column of Fig. 4 we compare measurements with theoretical predictions based on the time domain code[17] for solving the KZK equation (dashed lines). We have expanded the time axis by a factor of 2 in order to better see the comparisons between theory and experiment. The source condition used as an input to the numerical algorithm is the measured direct wave at $z=2$ mm in Fig. 4 (we deleted the edge wave). The small amount of ringing associated with turning the source on and off is also included, and we expect to see this effect also propagate as a part of our solution. Based on the source parameters ($f_0=2.25$ MHz, $a=9.4$ mm, and $p_0=274$ kPa) and the properties of fresh water ($\rho_0=998$ kg/m^3, $c_0=1486$ m/s, and $\beta=3.5$), the absorption and nonlinearity parameters are $N_u=1.72$ and $A_u=0.053$. We start the comparison at range $z/z_0=0.14$ ($z=60$ mm), and not any closer to the source because the theoretical model becomes increasingly inaccurate. Specifically, for a circular piston the parabolic approximation is valid on axis for[25] $z \gtrsim a(ka)^{1/3}$, which corresponds to $z \gtrsim 42$ mm for the parameters of our experiment. Errors introduced on axis by the parabolic approximation are associated with the arrival time of the edge wave. At $z/z_0=0.14$ the agreement between measurement and theory is good for the center wave, but less so for the edge wave. As we move further out, the edge wave catches up with the center wave, and at about $z/z_0=0.24$ the two signals overlap. After that range the wave distorts nonlinearly. The overall agreement between the mea-

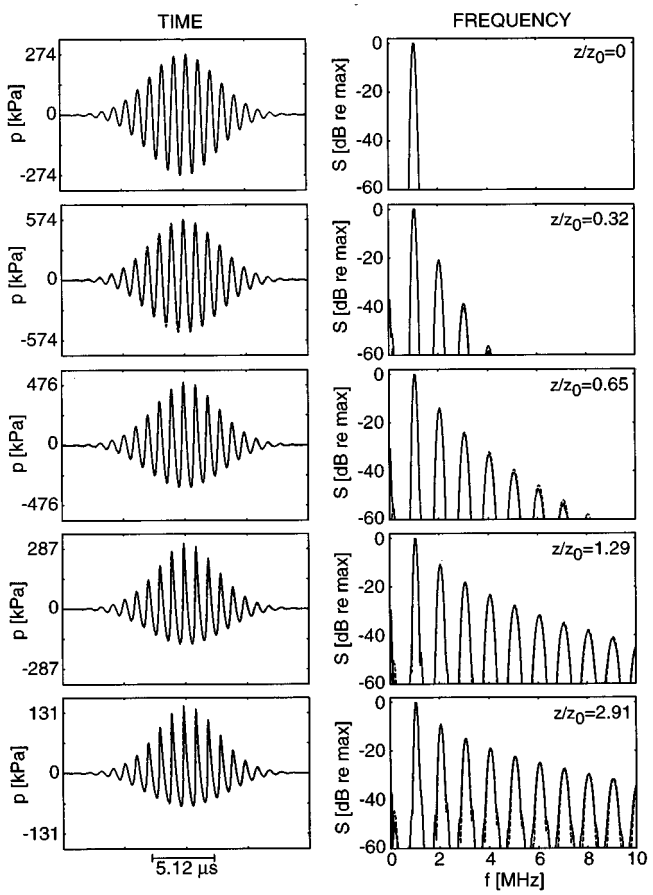

FIG. 5. Comparisons of measurements (solid lines; $f_0=1$ MHz, $a=12.1$ mm, $z_0=310$ mm) of a tone burst with Gaussian envelope ($\omega_0 T=16\pi$, $m=1$) along the axis of a plane piston with theory (dashed lines; $A_u=0.007$, $N_u=0.57$).

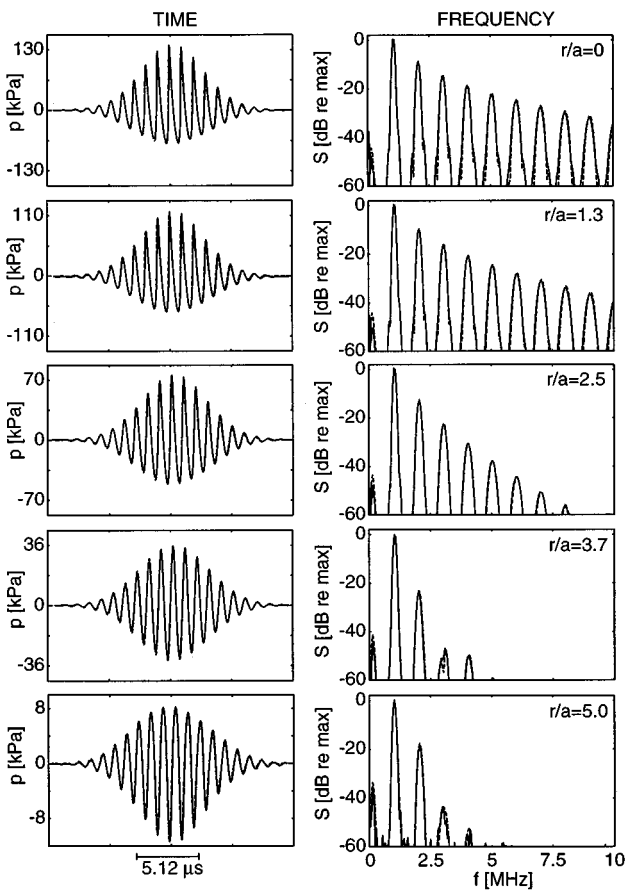

FIG. 6. Comparisons of measurements (solid lines) with theory (dashed lines) across the beam for the pulse in Fig. 5 at $z/z_0=2.91$.

surements and the theoretical predictions is very good.

We now present measurements of a Gaussian (envelope) tone burst radiated by the 1-MHz plane piston. Except for the first waveform (the source function), all measurements were made beyond the last near-field null in the propagation curve at 1 MHz. The values $\omega_0 T=16\pi$ and $m=1$ determined the relative duration and rise time of the pulse, respectively, and they defined the input functions for both the signal generator (LeCroy 9112 arbitrary function generator) and the theoretical calculations shown as dashed lines in Fig. 5. The absorption and nonlinearity parameters are $A_u=0.007$ and $N_u=0.57$, respectively. The left column in Fig. 5 contains the measured and calculated pressure waveforms $p(t')$, and the right column shows the corresponding spectral magnitudes S, which are obtained with a fast Fourier transform (FFT) of the time waveforms (both measured and calculated). Note that absolute pressures are provided for the time waveforms, whereas the frequency spectra are normalized by their peak values at the given location. At $z/z_0=0$ (at the source), we show the source condition that was supplied to both the function generator and the numerical solution. As the pulse propagates in water, the higher harmonic bands increase in level as expected, and the time waveforms distort. The agreement between measurement and theory is excellent (in fact, indistinguishable in the waveforms, although we note that the positive waveform peaks are slightly underpredicted by the theory and the negative peaks are overpredicted by equal amounts). We were limited to a maximum distance $z/z_0=2.91$ ($z=900$ mm) because of the size of the water tank.

Figure 6 contains measurements and theoretical predictions of the Gaussian pulse across the beam at range $z/z_0=2.91$, which corresponds to the range of the last waveform shown in Fig. 5. The left column shows the time waveforms and the right column the corresponding normalized frequency spectra, for both measurements and theoretical predictions. Since the higher harmonics are generated in narrower beams, we expect to see them decay more rapidly than the fundamental as we move off axis. Indeed, that is what happens in Fig. 6 from $r/a=0$ to $r/a=3.7$, in which region the distortion of the time waveforms diminishes accordingly (i.e., the shock front disappears). We note that linear theory predicts the first null in the far-field beam pattern at 1 MHz to occur at $r/a=5.6$.

In both Figs. 5 and 6 a nonlinearly generated low-frequency band (below the fundamental component) is seen. This frequency band is associated with self-demodulation.[26] As seen in Fig. 6, the low-frequency spectrum grows relative to the harmonics of the fundamental as we move off axis, because the low-frequency components have broader directivities. The agreement between measurements and numerical predictions for the low-frequency components is not

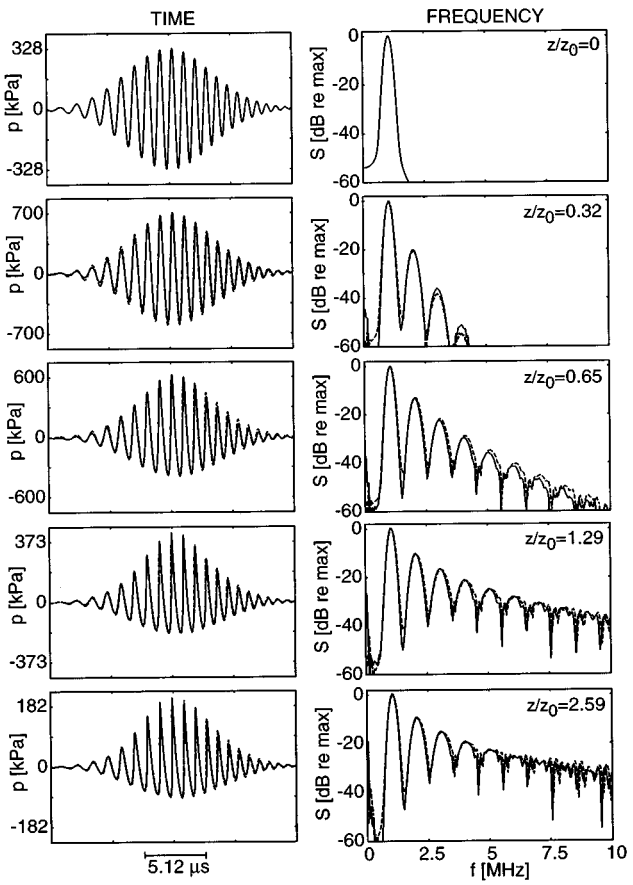

FIG. 7. Comparisons of measurements (solid lines; $f_0=1$ MHz, $a=12.1$ mm, $z_0=310$ mm) of a frequency modulated pulse having a Gaussian envelope $[\omega_0 T=16\pi,\ m=1,\ \phi(t)=(\omega_0 t)^2/120\pi]$ along the axis of a plane piston with theory (dashed lines; $A_u=0.007$, $N_u=0.684$).

quite as good as for the other components. A possible explanation is the receiver frequency response at low frequencies. It is known that the response of this type of hydrophone departs from ideal as the frequency is lowered below 1 MHz. Self-demodulation has been investigated in detail elsewhere,[27] with both theory and experiment, for the case of strong absorption.

Shown in Fig. 7 are axial measurements and theoretical predictions for a frequency-modulated Gaussian pulse with a center frequency of $f_0=1$ MHz and a phase modulation defined by $\phi(t)=(\omega_0 t)^2/120\pi$. The remaining source parameters are $\omega_0 T=20\pi$, $m=1$, $A_u=0.007$, and $N_u=0.684$. The instantaneous angular frequency of the tone is $\Omega/2\pi=(1+4f_0 t/120)f_0$, which increases linearly with time by approximately 50% over the duration of the pulse. As in Fig. 5, the waveform at $z=0$ represents the electrical input to the transducer, as well as the numerical input to the computer code. The general trends in Fig. 7 are the same as those in Fig. 5. However, the spectral bands are now wider because of the broader frequency band at the source, and at $z/z_0=2.59$ the high-frequency spectrum is very noiselike in appearance. The agreement between measurement and theory is again very good.

According to linear acoustical theory, the received sound pressure level at a fixed point increases linearly with

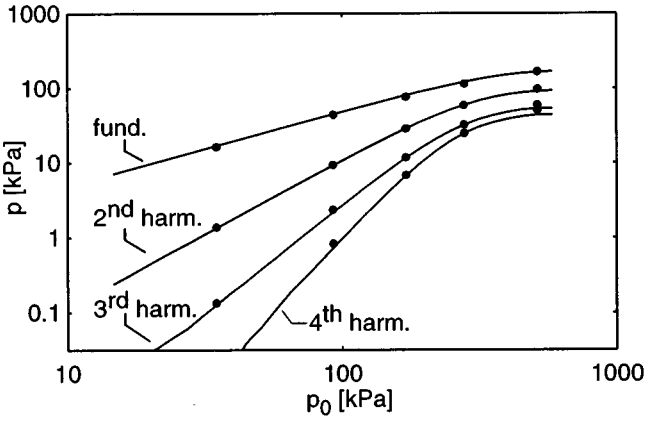

FIG. 8. Measurements (solid lines; $f_0=1$ MHz, $a=12.1$ mm, $z_0=310$ mm) and theoretical predictions (dots; $A_u=0.007$) of acoustic saturation of a finite amplitude tone burst ($\omega_0 T=34\pi$, $m=4$) in an unfocused beam at $z/z_0=2.3$.

increasing source level. At sufficiently high amplitudes, however, the amount of energy transmitted through a medium is limited by shock formation. The limit at which all additional energy supplied by the source is dissipated between the source and receiver is known as acoustic saturation. Acoustic saturation in cw fields has been investigated experimentally in the past, first for plane and spherical waves,[28,29] and subsequently for directional sound beams.[30,31] In Fig. 8 we compare theory and experiment for acoustic saturation associated with a pulsed sound beam.

With the source function defined by $\omega_0 T=34\pi$ and $m=4$, the amplitude of the 1-MHz transducer was increased while the axial sound pressure at $z=700$ mm ($z/z_0=2.3$) was monitored with the hydrophone. The peak amplitudes of the lowest four frequency bands were then plotted, solid lines for measurements and circles for theory. For each source level at which we ran the computer code, we took an additional three measurements along the axis of the source and compared them with theory to ensure that the complete field was accurately modeled along the entire propagation path. The agreement between experiment and theory was equally good at all amplitudes. Acoustic saturation is one case in which experiments are easier to perform than are the calculations. For reference, in Fig. 5 the source pressure was 274 kPa, and it corresponds to the fourth (from left) theoretical point in Fig. 8, which marks the onset of acoustic saturation. The distance at which the measurements were made for Fig. 8 was 700 mm ($z/z_0=2.3$), which corresponds to waveform distortion at an intermediate stage between the last two waveforms of Fig. 5.

B. Focused pistons

The focused 2.25-MHz piston ($G=10.5$) described in Sec. II was used in all experiments reported in the present section.

The measured waveforms in Fig. 9 were created by using the parameters $\omega_0 T=14\pi$ and $m=2$ to define the input function for the signal generator. The source waveform used in the theoretical calculations is the measured direct wave at

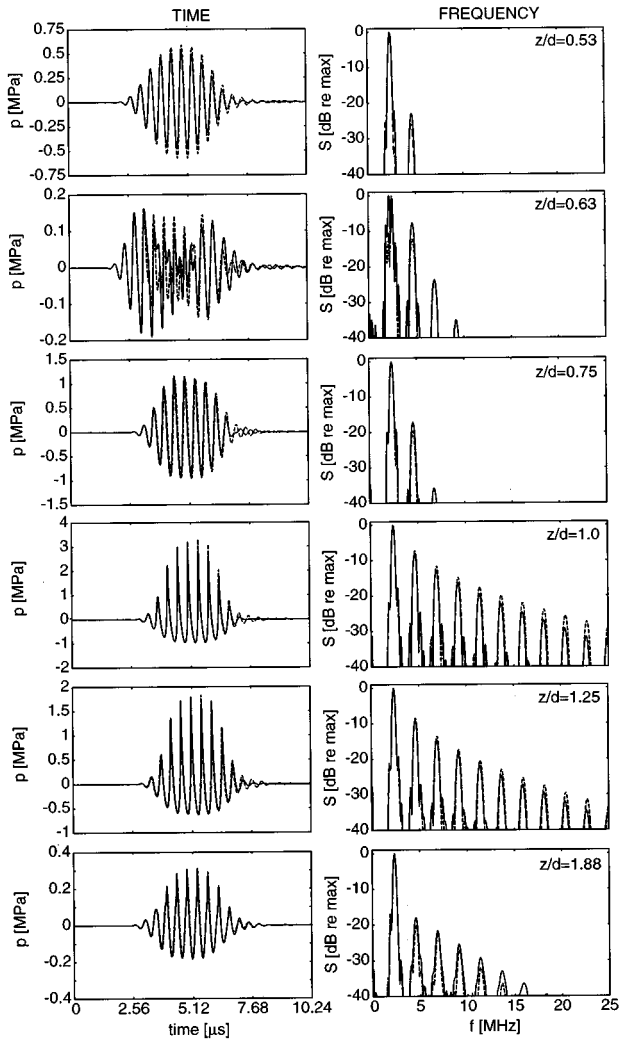

FIG. 9. Comparisons of measurements (solid lines; $f_0=2.25$ MHz, $a=18.8$ mm, $d=160$ mm) of a tone burst ($\omega_0 T=14\pi$, $m=2$) with theory (dashed lines; $A_f=0.025$, $N_f=0.34$, $G=10.5$) along the axis of a focused piston.

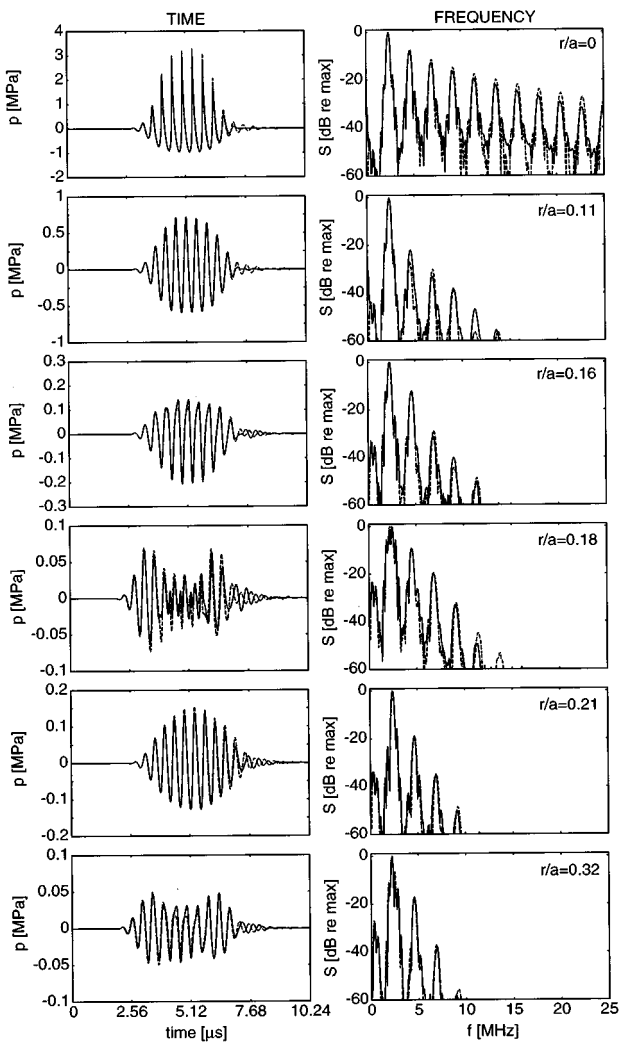

FIG. 10. Comparisons of measurements (solid lines) with theory (dashed lines) across the beam for the pulse in Fig. 9 at $z/d=1.0$.

$z=10$ mm ($z/d=0.06$, not shown). For a focused circular piston, the pressure field along the axis is also composed of two replicas of the incident waveform, as with the plane piston (see discussion of Fig. 3). However, the two contributions arrive at the same time only at the focus. In the prefocal region the direct wave precedes the diffracted wave, whereas in the postfocal region the diffracted wave arrives first. At $z=10$ mm the center and edge waves were separated completely by about three cycles. The absorption and nonlinearity parameters are $A_f=0.025$ and $N_f=0.34$, respectively.

The left column in Fig. 9 contains the measured and calculated pressure waveforms $p(t')$, and the right column shows the corresponding normalized spectral magnitudes S obtained by taking the FFT of $p(t')$. The range $z/d=0.53$ corresponds to a prefocal maximum in the propagation curve at 2.25 MHz, where the waveform closely resembles the signal at the source. The range $z/d=0.63$ corresponds to the last prefocal null, where the direct wave and edge wave differ by almost 180° and thus cancel in the center of the pulse. The apparent increase in the duration of the waveform at $z/d=0.63$ in comparison with the waveforms presented just above and below is due in part to the magnified scale that was used to compensate for the reduction in amplitude due to phase cancellation. As the pulse propagates towards the focus the amplitude increases, the higher harmonic bands increase in level, and the time waveforms distort. Beyond the focus the waveforms decrease in amplitude and become less distorted. At the focus, the agreement of theory with experiment worsens with increasing frequency. The difference between experiment and theory is less than 1 dB for the first four harmonics and it increases to about 3 dB at the tenth harmonic. The increasing discrepancies at the higher harmonics may be attributed to spatial averaging because the beamwidths become comparable to the diameter of the active element of the hydrophone.

Figure 10 contains measurements (solid lines) and theoretical predictions (dashed lines) of a pulse with the same parameters as in Fig. 9, at positions across the beam in the focal plane ($z/d=1.0$). The left column shows the time waveforms and the right column the corresponding normalized frequency spectra. The positions $r/a=0.18$ and $r/a=0.32$ correspond to nulls predicted by linear theory at 2.25

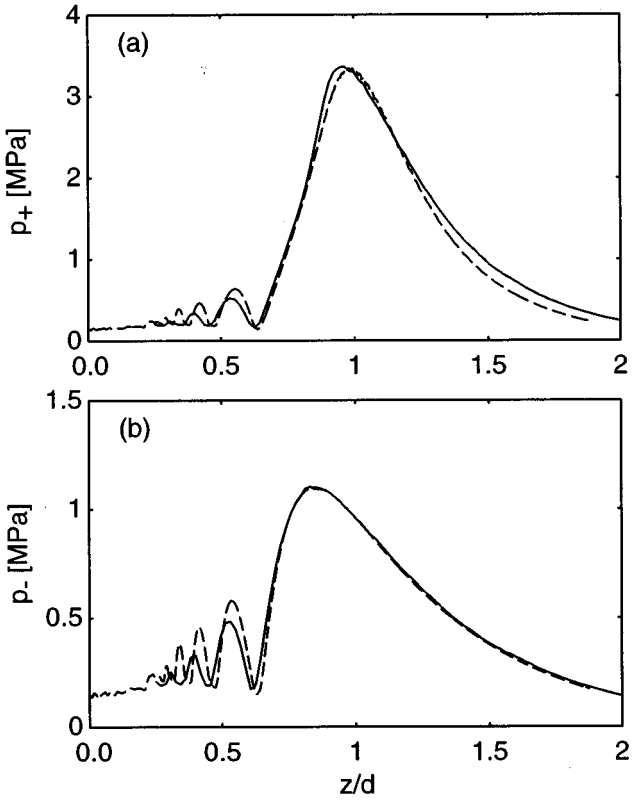

FIG. 11. Comparison of measurements (solid lines; $f_0=2.25$ MHz, $a=18.8$ mm, $d=160$ mm) and theory (dashed lines; $A_f=0.025$, $N_f=0.34$, $G=10.5$) of the axial peak positive (a) and negative pressures (b) of the pulse in Fig. 9.

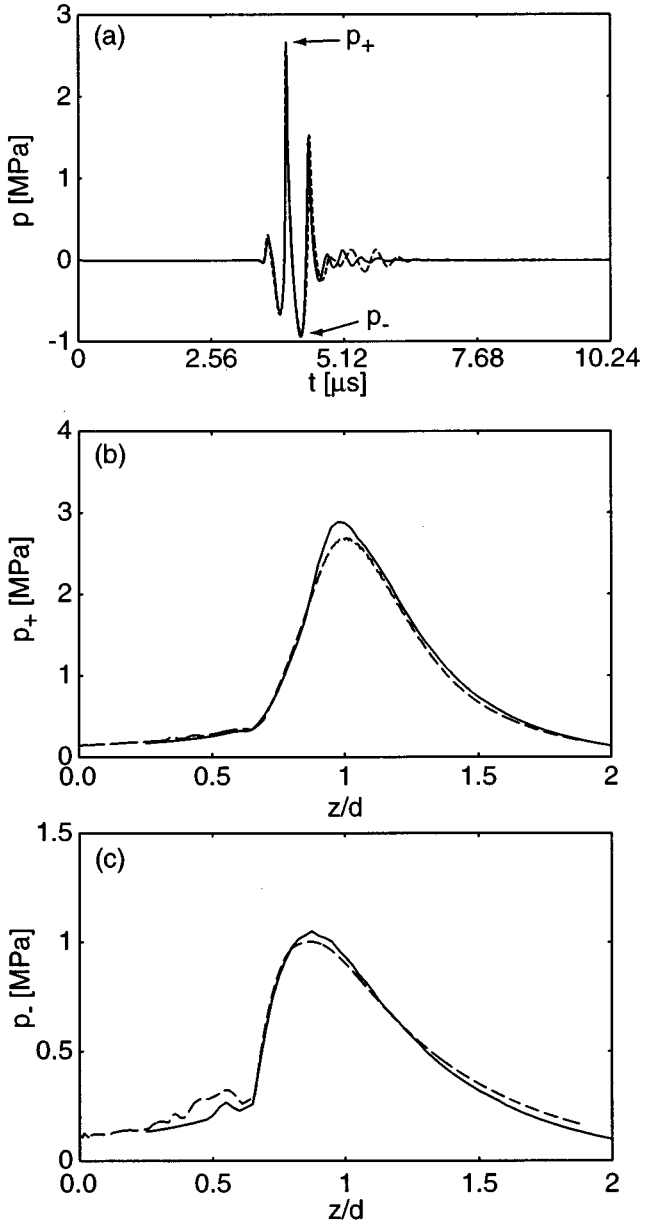

FIG. 12. Comparison of measurements (solid lines; $f_0=2.25$ MHz, $a=18.8$ mm, $d=160$ mm) and theory (dashed lines; $A_f=0.025$, $N_f=0.35$, $G=10.5$) for the axial waveform at the focus (a) and the propagation curves of the peak positive (b) and negative pressures (c) of a short pulse.

MHz, the center frequency of the source waveform. Note also the nonlinearly generated low-frequency band, below the primary frequency band. Low-pass filtering of the waveforms shown in Fig. 10 reveals a waveform that resembles the second derivative of the square of the pulse envelope.

Axial propagation curves of the peak positive (p_+) and negative (p_-) pressures for the pulse shown in Fig. 9 are shown in Fig. 11. The measurements are shown as solid lines and the theoretical predictions as dashed lines. We note that the maximum value of p_+ occurs very close to the geometric focus of the source ($z/d\simeq 1.0$). However, p_- is maximized earlier ($z/d\simeq 0.8$), the significance of which is that the negative pressure plays an important role in acoustic cavitation. In medical ultrasound applications where cavitation activity may be deleterious, special care must be given to monitor cavitation in the prefocal region. *In vitro* and *in vivo* experiments[32,33] that show increased cavitation activity in the prefocal region of a lithotripter are in agreement with our results. The numerical model described here has been applied to lithotripsy fields[34,35] as well, where higher amplitudes and broader frequency pulses are utilized and similar observations have been noted.

The comparisons shown in Fig. 11 were repeated for a much shorter pulse (about 2 cycles), and these results are presented in Fig. 12. Figure 12(a) shows the measured waveform and the theoretical prediction at the focus. Comparisons of measurements and theory for the propagation curves of p_+ and p_- are shown in Fig. 12(b) and (c), respectively. Note that the negative pressure is maximized in the prefocal region, whereas the positive pressure is maximized closer to the geometric focus. A difference between Figs. 11 and 12 is that the near-field diffraction oscillations in Fig. 11 are not seen in Fig. 12 because of the shorter pulse length.

Shown in Fig. 13 are propagation curves for p_+ and p_- with $p_0=28.4$, 85.2, 142, and 189 kPa. The values $\omega_0 T=14\pi$ and $m=2$ determined the relative duration and rise time of the pulse (same source function parameters as in Fig. 9). The peak positive pressure is maximized close to $z/d=1$, with the exception of the case with $p_0=189$ kPa, for which there is a prefocal shift. A very slight prefocal shift is also seen for the 142 MPa pressure. This shift may be due to

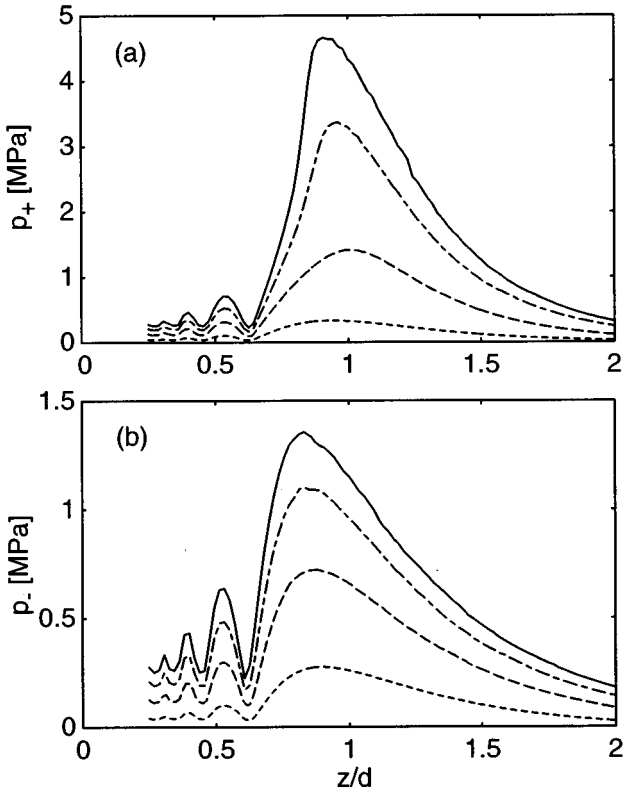

FIG. 13. Measurements of the peak positive (p_+) and negative pressures (p_-) along the axis of a focused piston ($f_0=2.25$ MHz, $a=18.8$ mm, $d=160$ mm) as function of source pressure: $p_0=28.4$, 85.2, 142, and 189 kPa, in bottom to top order.

bandwidth limitations of the hydrophone which, for the large pressure amplitudes involved ($p_+>3$ MPa), introduce uncertainty in the observed spikes associated with the peak shock pressures. Since the corresponding waveforms contained strong shocks and thus had a frequency content that extended beyond the frequency response of the hydrophone, they contained a fair amount of ringing. The maximum value of p_- is located clearly before the focus and shifts closer to the source with increasing source pressure. Errors due to hydrophone frequency response are not easily observed with measurements of p_- because the rarefaction phase of the waveform is less sensitive to measurement bandwidth than the compression phase.

IV. CONCLUSION

Detailed measurements of pulses radiated by plane and focused circular pistons in water have been shown. Emphasis was placed on nonlinear distortion of pulses. The measurements exhibit high spatial resolution and extend over a dynamic range of up to 80 dB. Thus, they enabled very precise comparisons to be made with numerical calculations based on the KZK equation. In particular, detailed comparisons of theory and experiment were made of waveforms and their corresponding spectra. The predictions are based on a time-domain algorithm for solving the KZK equation. This time-domain approach is particularly suitable for modeling pulses, and short transients in general. Acoustic saturation of a pulse was investigated. Axial propagation curves of the peak negative pressure (p_-) of an ultrasonic pulse radiated by a focused piston source indicate that the maximum negative pressure occurs in the prefocal region, a result that is relevant to acoustic cavitation studies. Finally, increasing the source pressure results in shifting of the maximum p_- closer to the source.

ACKNOWLEDGMENTS

This work was supported by the Office of Naval Research, the David and Lucile Packard Foundation Fellowship for Science and Engineering, and the National Institutes of Health (Grant No. DK-43881).

[1] A. J. Coleman and J. E. Saunders, ''A review of the physical properties and biological effects of the high amplitude acoustic fields used in extracorporeal lithotripsy,'' Ultrasonics **31**, 75–89 (1993).
[2] D. A. Hutchins and G. Hayward, ''Radiated fields of ultrasonic transducers,'' in *Ultrasonic Measurement Methods*, Vol. 19 of *Physical Acoustics*, edited by R. N. Thurston and A. D. Pierce (Academic, New York, 1990), pp. 1–80.
[3] M. M. Goodsitt, E. L. Madsen, and J. A. Zagzebski, ''Field patterns of pulsed, focused, ultrasonic radiators in attenuating and nonattenuating media,'' J. Acoust. Soc. Am. **71**, 318–329 (1982).
[4] H. Djelouah, J. C. Baboux, and M. Perdix, ''The transient field of a planar ultrasonic transducer coupled to a lens: Experiments and simulations,'' J. Acoust. Soc. Am. **87**, 76–80 (1990).
[5] H. Djelouah, J. C. Baboux, and M. Perdix, ''Theoretical and experimental study of the field radiated by ultrasonic focused transducers,'' Ultrasonics **29**, 188–200 (1991).
[6] A. C. Baker and V. F. Humphrey, ''Distortion and high-frequency generation due to nonlinear propagation of short ultrasonic pulses from a plane circular piston,'' J. Acoust. Soc. Am. **92**, 1699–1705 (1992).
[7] A. C. Baker and V. F. Humphrey, ''Nonlinear propagation of short ultrasonic pulses in focused fields,'' in *Frontiers of Nonlinear Acoustics: Proceedings of 12th ISNA*, edited by M. F. Hamilton and D. T. Blackstock (Elsevier Applied Science, London, 1990), pp. 185–190.
[8] A. C. Baker and V. F. Humphrey, ''Nonlinear propagation in pulsed ultrasonic transducers,'' in *Proceedings of Ultrasonics International 89* (Butterworth, London, 1989), pp. 691–696.
[9] E. A. Zabolotskaya and R. V. Khokhlov, ''Quasi-plane waves in the nonlinear acoustics of confined beams,'' Sov. Phys. Acoust. **15**, 35–40 (1969).
[10] V. P. Kuznetsov, ''Equation of nonlinear acoustics,'' Sov. Phys. Acoust. **16**, 467–470 (1970).
[11] R. E. Apfel and C. K. Holland, ''Gauging the likelihood of cavitation from short-pulse, low duty cycle diagnostic ultrasound,'' Ultrasound Med. Biol. **17**, 179–185 (1991).
[12] J. Lighthill, *Waves in Fluids* (Cambridge U.P., Cambridge, 1980), pp. 78–83.
[13] D. T. Blackstock, ''Nonlinear Acoustics (Theoretical),'' in *American Institute of Physics Handbook* (McGraw-Hill, New York, 1972), 3rd ed., Chap. 3n.
[14] E. H. Vefring, J. Naze Tjøtta, and S. Tjøtta, ''Effects of focusing on the nonlinear interaction between two collinear finite amplitude sound beams,'' J. Acoust. Soc. Am. **89**, 1017–1027 (1991).
[15] J. Naze Tjøtta, S. Tjøtta, and E. H. Vefring, ''Propagation and interaction of two collimated finite amplitude sound beams,'' J. Acoust. Soc. Am. **88**, 2859–2870 (1990).
[16] J. Naze Tjøtta and S. Tjøtta, ''Nonlinear equations of acoustics, with application to parametric acoustic arrays,'' J. Acoust. Soc. Am. **69**, 1644–1652 (1981).
[17] Y. S. Lee and M. F. Hamilton, ''Time-domain modeling of pulsed finite-amplitude sound beams,'' J. Acoust. Soc. Am. **97**, 906–917 (1995).
[18] R. O. Cleveland, M. F. Hamilton, and D. T. Blackstock, ''Time-domain modeling of finite-amplitude sound in relaxing fluids,'' J. Acoust. Soc. Am. **99**, 3312–3318 (1996).
[19] Y.-S. Lee, ''Numerical solution of the KZK equation for pulsed finite amplitude sound beams in thermoviscous fluids,'' Ph.D. dissertation, The University of Texas at Austin, 1993.

[20] J. A. TenCate, ''An experimental investigation of the nonlinear pressure field produced by a plane circular piston,'' J. Acoust. Soc. Am. **94**, 1084–1089 (1993).
[21] M. A. Averkiou, ''Experimental investigation of propagation and reflection phenomena in finite-amplitude sound beams,'' Ph.D. dissertation, The University of Texas at Austin, 1994, Appendix A.
[22] M. A. Averkiou and M. F. Hamilton, ''Measurements of harmonic generation in a focused finite-amplitude sound beam,'' J. Acoust. Soc. Am. **98**, 3439–3442 (1995).
[23] D. R. Bacon, ''Characteristics of a pvdf membrane hydrophone for use in the range 1–100 MHz,'' IEEE Trans. Sonics Ultrason. **SU-29**, 18–25 (1982).
[24] B. J. Landsberger, ''Second harmonic generation in sound beams reflected from and transmitted through immersed elastic solids,'' Ph.D. dissertation, The University of Texas at Austin, 1997, Appendix C.
[25] J. Naze Tjøtta and S. Tjøtta, ''An analytical model for the nearfield of a baffled piston transducer,'' J. Acoust. Soc. Am. **68**, 334–339 (1980).
[26] H. O. Berktay, ''Possible exploitation of non-linear acoustics in underwater transmitting applications,'' J. Sound Vib. **2**, 435–461 (1965).
[27] M. A. Averkiou, Y.-S. Lee, and M. F. Hamilton, ''Self-demodulation of amplitude- and frequency-modulated pulses in a thermoviscous fluid,'' J. Acoust. Soc. Am. **94**, 2876–2883 (1993).
[28] C. H. Allen, ''Finite amplitude distortion in a spherically diverging sound wave in air,'' Ph.D. dissertation, Pennsylvania State University, 1950.
[29] D. A. Webster and D. T. Blackstock, ''Finite-amplitude saturation of plane sound waves in air,'' J. Acoust. Soc. Am. **62**, 518–523 (1977).
[30] J. A. Shooter, T. G. Muir, and D. T. Blackstock, ''Acoustic saturation of spherical waves in water,'' J. Acoust. Soc. Am. **55**, 54–62 (1974).
[31] T. L. Riley, ''Generation of harmonics in finite amplitude sound radiated in water by a circular piston,'' M.S. thesis, The University of Texas at Austin, 1983.
[32] A. J. Coleman, M. Whitlock, T. Leighton, and J. E. Saunders, ''The spatial distribution of cavitation induced acoustic emission, sonoluminescence and cell lysis in the field of a shock wave lithotripter,'' Phys. Med. Biol. **38**, 1545–1560 (1993).
[33] A. J. Coleman, T. Kadama, M. J. Choi, T. Adams, and J. E. Saunders, ''The cavitation threshold of human tissue exposed to 0.2 MHz pulsed ultrasound: Preliminary measurements based on a study of clinical lithotripsy,'' Ultrasound Med. Biol. **21**, 405–417 (1995).
[34] M. A. Averkiou, L. A. Crum, and M. F. Hamilton, ''Theoretical modeling of the acoustic pressure field produced by commercial lithotripters,'' J. Acoust. Soc. Am. **98**, 2941(A) (1995).
[35] M. A. Averkiou and L. A. Crum, ''Cavitation: Its role in stone comminution and renal injury,'' in *Topics in Clinical Urology: New Developments in the Management of Urolithiasis*, edited by J. Lingeman and G. M. Preminger (Igaku-Shoin Medical Publishers, New York, 1995), pp. 21–40.